Revisiting the Three-Vanadium Sandwich Type Polyoxometalates: Structures, Solution Behavior and Redox Properties

Ibrahima Fa Bamba, Clément Falaise, Jérôme Marrot, Gildas K Gbassi, Patrick Atheba, Régis Guillot, Mohamed Haouas, Emmanuel Cadot

Revisiting the Three-Vanadium Sandwich Type Polyoxometalates: Structures, Solution Behavior and Redox Properties

Ibrahima Fa Bamba,[a] Clément Falaise,[a] Jérôme Marrot,[a] Gildas K. Gbassi,[b] Patrick Atheba,[c] Regis Guillot,[d] Mohamed Haouas,[a] and Emmanuel Cadot[a]**

a) Institut Lavoisier de Versailles, CNRS, UVSQ, Université Paris-Saclay, Versailles, France
b) UFR Sciences Pharmaceutiques et Biologiques (UFR SPB), Université Félix Houphouët Boigny (UFHB), Abidjan, Côte d'Ivoire
c) UFR Sciences des Structures de la Matière et Technologie (UFR SSMT), Université Félix Houphouët Boigny (UFHB), Abidjan, Côte d'Ivoire
d) Institut de Chimie Moléculaire et des Matériaux d'Orsay, CNRS, Université Paris Sud, Université Paris Saclay, 91405 Orsay Cedex, France

ABSTRACT. It is well-known that the trivacant anions α-B-$[XW_9O_{33}]^{9-}$ react with vanadyl ions to give the sandwich type polyoxometalates $[(V^{IV}O)_3(XW_9O_{33})_2]^{12-}$ with X = As^{III} or Sb^{III}. Nevertheless, the oxidized derivatives have been obtained selectively by electrochemical oxidation from the fully reduced derivatives $[(V^{IV}O)_3(XW_9O_{33})_2]^{12-}$ allowing full characterization both in solution using UV-vis and multinuclear (^{17}O, ^{51}V, ^{183}W) NMR spectroscopies, and in the solid-state by single-crystal X-ray diffraction. Structural analysis of the oxidized $[(V^{V}O)_3(XW_9O_{33})_2]^{9-}$ polyanions is consistent with the idealized D_{3h} symmetry while solution studies reveal a fair hydrolytic stability in a wide *p*H range from 0 to 6. Besides, the D_{3h} polyanions either as reduced or oxidized forms $[(VO)_3(AsW_9O_{33})_2]^{9/12-}$ has been identified as the thermodynamic product that results from the conversion of the C_{2v} polyanion $[(H_2O)(VO)_3(AsW_9O_{33})_2]^{9/12-}$ through moderate heating. Conversely, the Sb^{III}-containing derivative gives exclusively the D_{3h} polyanion, probably due either to the extended lone pair of the trigonal Sb^{III} heterogroup that prevents the formation of the C_{2v} arrangement or to the lability of the oxo-metalate bonds that favors chemical exchange. The electrochemical studies of sandwich type polyoxometalates revealed that each {V=O} group gives rise to a one-electron transfer process. At last, the redox properties appear strongly altered in the 0.3 – 5 *p*H range, consistent with proton-coupled electron transfers (PCET).

INTRODUCTION

Polyoxometalates (POMs) represent a class of water-soluble metal-oxo clusters built from group V and VI transition metals in their highest oxidation states (V^{V}, Nb^{V}, Ta^{V}, Mo^{VI} or W^{VI}).[1] This class of water-soluble polyanions exhibits a wide diversity of structures and compositions which opened new avenues toward potential applications in various fields including catalysis, medicine, materials science and energy storage and conversion.[2–6] Mo^{VI} or W^{VI}-based POM entities containing vanadium addenda attract attention because of their excellent performances in homogeneous and heterogeneous oxidation catalysis for conversion of organic substrates.[7–13] Most of the mixed V/W and V/Mo POMs exhibit archetypal architectures such as Lindqvist, Keggin or Dawson type arrangements.[14–20] These mixed-metal compounds are usually obtained from aqueous solution through stereo-selective addition of vanadium oxo-based species on vacant polyoxometalates containing tetrahedral heteroatoms such as P^{V} or Si^{IV}. However, the use of B-type trivacant Keggin derivatives having trigonal heteroatoms (As^{III}, Sb^{III}, Bi^{III}, Se^{IV} or Te^{IV}) favors the formation of sandwich type assemblies[21–27] or more complex high nuclearity arrangements.[28–30] It is well-admitted that the presence of lone pair of electrons on the heteroatom avoids the formation of closed-shell Keggin anions.[31]

Then, these basic sandwich type assemblies exhibit three metal centers inserted between two {α-B-XW_9O_{33}} units. This structural arrangement, sometimes called Hervé-type POM has been isolated with various metal centers including divalent transition metals (M^{II}),[21,32–36] mixed metals ($2V^{V}/Ln^{III}$, $2Ti^{IV}/M^{II}$),[37–39] organo-antimony entities,[40] Nb^{V} or W^{VI}.[41,42] The vanadium-containing Hervé-type POM can exhibit various V^{V}/V^{IV} oxidation[18–21] leading to interesting magnetic behavior[21,23,43–45] or antiviral properties[45,46]. Structural characterization of $[(VO)_3(SbW_9O_{33})_2]^{12-}$ and $[(VO)_3(BiW_9O_{33})_2]^{12-}$ anions shows three square pyramidal vanadium centers featured by a terminal {V^{IV}=O} bonds, all directed toward the exterior of the POM, forming a D_{3h} sandwich-type POMs (Figure 1).[22–24] The situation appears much more intricate for the As^{III} derivatives. For instance, Mialane et *al*. observed the possible existence of a C_{2v} metal-oxo framework, disordered with the D_{3h} species in the crystal.[21] This latter is characterized by one V=O bond directed toward the center of the central closed cavity, while the two other {V=O} groups remain outward-directed (Figure 1). Actually, the formation of two entities should be dependent upon either the

synthetic/crystallization procedures or the nature of the hetero-elements (e.g. As^{III} versus Sb^{III}). It is worthy to mention that the C_{2v} arrangement is not limited to vanadium based POM but can be extended to {W=O} groups in $[(H_2O)(WO)_3(AsW_9O_{33})_2]^{6-}$ anion and even to the {Zn-OH_2} distribution in $[(Zn(H_2O))_3(XW_9O_{33})_2]^{12-}$ with X = As^{III} or Sb^{III}.[33,42]

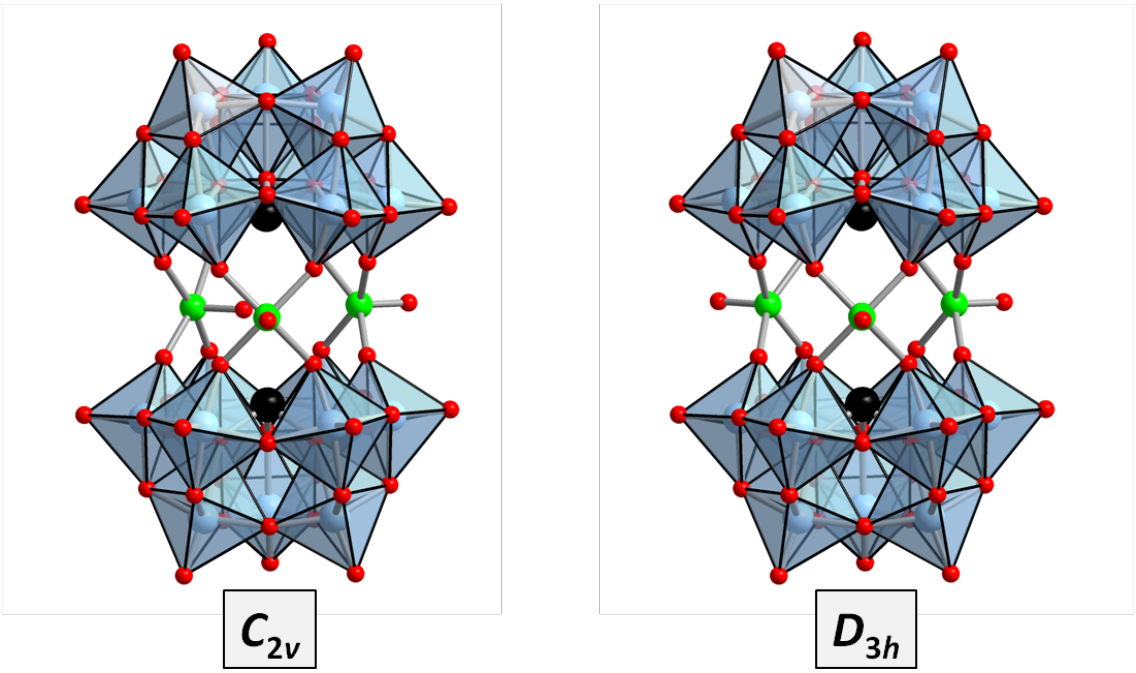

Figure 1: Polyhedral representation of the metal-oxo core of the three vanadium-containing Hervé-type POMs that can adopt a D_{3h} or C_{2v} symmetry depending on the orientation of the V=O bond within the {V_3} triangle. Color code: cyan octahedra: WO_6; green sphere: vanadium; red sphere: oxygen; black sphere: lone pair containing heteroatom (X = As^{III}, Sb^{III} or Bi^{III}).

In this contribution, we report first the preparation and structural characterization of two Hervé-type POMs built from two $[AsW_9O_{33}]^{9-}$ subunits, showing that the C_{2v} species corresponds mostly to the kinetic product which converts itself into the D_{3h} entity, identified as the thermodynamic species. In contrast, using the preformed unit $[SbW_9O_{33}]^{9-}$ systematically led to the D_{3h} species. Then, we report the electrochemical preparation of the fully oxidized V^V containing $[(VO)_3(XW_9O_{33})_2]^{9-}$ anions. The resulting diamagnetic compounds were characterized both in solution by multinuclear NMR (^{17}O, ^{51}V and ^{183}W) and in the solid-state by X-ray diffraction. The hydrolytic stability and electrochemical behavior of these oxidized Hervé-type POMs (D_{3h} species) have been investigated in aqueous solutions. These investigations evidence the three vanadium centers undergo one-electron transfer through *p*H-dependent processes. In acidic condition, the

single redox wave is consistent with a quasi-reversible three-electron exchange, while at higher *p*H, the single wave splits into three successive mono-electronic transfers.

EXPERIMENTAL SECTIONS

Materials. All chemicals were used as received without any further treatment. Trivacant Keggin anions $Na_9[\alpha\text{-}AsW_9O_{33}]\bullet 19.5H_2O$ and $Na_9[\alpha\text{-}SbW_9O_{33}]\bullet 19.5H_2O$ used as precursors were synthetized according to the literature.[47,48] The preparation of the fully reduced forms has been carried out under nitrogen to avoid any oxidation of vanadyl ions.

Preparation of the reduced derivative $[(H_2O)(VO)_3(AsW_9O_{33})_2]^{12-}$ (notated $\mathbf{1^{red}}.\boldsymbol{C_{2v}}$). Under vigorous stirring, 22.52 g (8 mmol) of $Na_9[AsW_9O_{33}]\cdot 19.5H_2O$ was added to an aqueous solution containing $VOSO_4\cdot 5H_2O$ (3 g, 12 mmol) in 160 mL of CH_3CO_2Na/CH_3CO_2H (0.5 M/0.5 M). The *p*H of the solution is about 4.5. The dark-brown resulting solution was stirred for 15 minutes at room temperature. Then, 15 g of RbCl is added, provoking immediately the precipitation of about brownish solid (19 g) that is recovered by filtration. The dissolution of 6 g of this brownish solid in 200 mL of aqueous NaCl solution (0.5 M), had led to well-shaped crystals of $H_{1.25}Rb_{4.75}Na_6[(H_2O)(VO)_3(AsW_9O_{33})_2]\cdot 15H_2O$ ($\mathbf{1^{red}}.\boldsymbol{C_{2v}}$) after evaporation (1 day). Yield: 62 % based on W. IR: 721, 742, 860, 900, 945, 968, 993, 1010 cm^{-1}. Anal. Calcd. (%) for $W_{18}V_3As_2Rb_{4.75}Na_6H_{33.25}O_{85}$: Rb, 7.3; Na, 2.5 V, 2.8; As, 2.7; W, 59.6. Found: Rb, 7.1; Na, 2.2 V, 2.9; As, 2.5; W, 60.6.

Preparation of the reduced derivatives $[(VO)_3(XW_9O_{33})_2]^{12-}$ with X = As^{III} and Sb^{III}. Under vigorous stirring, 22.52 g (8 mmol) of $Na_9[AsW_9O_{33}]\cdot 19.5H_2O$ was added to an aqueous solution containing $VOSO_4\cdot 5H_2O$ (4 g, 16 mmol) in 160 mL of CH_3CO_2Na/CH_3CO_2H (0.5 M/0.5 M). The *p*H of the solution is about 4.5. The dark-brown resulting solution was then heated at 70-80 °C for 12 h and filtered off. After cooling at room temperature 30 g KCl was added, leading to brown solids. 19 g of $H_{1.5}K_{10.5}[(VO)_3(AsW_9O_{33})_2]\cdot 20H_2O$ (notated $\mathbf{1^{red}}.\boldsymbol{D_{3h}}$) is recovered by filtration under vacuum and then washed with ethanol (50 mL) and diethylether (50 mL). Yield: 84 % based on W. Crystals suitable for single-crystal analysis have been obtained by recrystallization in water. IR: 727, 750, 876, 900, 944, 986 cm^{-1}. Anal. Calcd. (%) for $W_{18}V_3As_2K_{10.5}H_{41.5}O_{89}$: K, 7.5; V, 2.8; As, 2.7; W, 60.3. Found: K, 6.9; V, 2.6; As, 2.6; W, 61.1. The compound

$H_{1.5}K_{10.5}[(VO)_3(SbW_9O_{33})_2]\cdot 20H_2O$ (notated $\mathbf{2^{red}}\boldsymbol{D_{3h}}$) has been isolated using similar synthetic procedure, except that the reaction was performed at room temperature. 22.52 g (8 mmol) of $Na_9[SbW_9O_{33}]\cdot 19.5H_2O$ have been added to obtained 18 g of $H_{1.5}K_{10.5}[(VO)_3(SbW_9O_{33})_2]\cdot 20H_2O$. The yield was 79 % based on W. IR: 690, 730, 854, 900, 944, 986 cm^{-1}. Anal. Calcd. (%) for $W_{18}V_3Sb_2K_{10.5}H_{41.5}O_{89}$: K, 7.4; V, 2.7; Sb, 4.4, W 59.2. Found: K, 7.2; V, 2.6; Sb, 4.0 W, 58.1.

Electrochemical preparation of the oxidized derivatives $[(VO)_3(XW_9O_{33})_2]^{9-}$ with X = As^{III}, and Sb^{III}. The electrochemical oxidations were carried out with a VersaSTAT 3 Potentiostat Galvanostat driven by a PC with the VersaStudio software. The three-electron-oxidized species were prepared from solutions of reduced anions $[(VO)_3(XW_9O_{33})_2]^{12-}$ by electrochemical oxidation at a controlled potential of carbon electrode. Typically, solutions of reduced anions were prepared from a 70 mL of CH_3CO_2Na/CH_3CO_2H buffer solution (0.5 M/0.5 M; *p*H = 4.8) in which 5 g of $\mathbf{1^{red}}\boldsymbol{D_{3h}}$ or $\mathbf{2^{red}}\boldsymbol{D_{3h}}$ were dissolved. The solids $K_9[(VO)_3(AsW_9O_{33})_2]\cdot 16H_2O$ (notated $\mathbf{1^{ox}}\boldsymbol{D_{3h}}$) and $K_9[(VO)_3(SbW_9O_{33})_2]\cdot 16H_2O$ (notated $\mathbf{2^{ox}}\boldsymbol{D_{3h}}$) have been precipitated by adding KCl (30 g) to the solutions of oxidized species. 4 g of yellow solids are recovered by filtration under vacuum and then washed with ethanol (20 mL) and diethylether (20 mL). Crystals suitable for single-crystal analysis have been obtained by recrystallization in water. IR of $\mathbf{1^{ox}}\boldsymbol{D_{3h}}$: 717, 754, 880, 912, 960, 992 cm^{-1}. Anal. Calcd. (%) for $W_{18}V_3As_2K_9H_{32}O_{85}$: K, 6.6; V, 2.8; As, 2.8; W, 61.8. Found: K, 6.4; V, 2.9; As, 3.0; W, 62.8. IR of $\mathbf{2^{ox}}\boldsymbol{D_{3h}}$: 685, 730, 870, 910, 960, 992 cm^{-1}. Anal. Calcd. (%) for $W_{18}V_3Sb_2K_9H_{32}O_{85}$: K, 6.5; V, 2.8; Sb, 4.5; W, 60.7. Found: K, 6.3; V, 2.9; Sb, 4.1; W, 60.9.

Electrochemical behavior. Cyclic voltammetric (CV) experiments were carried out with a PalmSens 4 driven by a PC with the PSTrace software. Measurements were performed at room temperature in a conventional single compartment cell. A glassy carbon (GC) electrode with a diameter of 2 mm was used as the working electrode. The auxiliary electrode was a Pt plate placed within a fritted-glass isolation chamber and potentials are quoted against Ag/AgCl electrode. The solutions were deaerated thoroughly for at least 10 minutes with pure argon and kept under a positive pressure of this gas during the experiments.

NMR studies. Spectra were recorded on Bruker Avance 400 and 500 MHz spectrometers using D_2O as lock solvent in standard 10 mm NMR tubes and fixing sample volume to 3 mL. Typically, ^{183}W NMR spectra were obtained accumulating 32k scans and using 2 s acquisition time, 1 s

relaxation delay, and 37 μs pulse length (π/2 flip angle). ^{51}V NMR spectra were recorded with 4k numbers of scans, 80 ms acquisition time, 0.1 s relaxation delay, and 1.3 μs pulse length (π/16 flip angle). The ^{17}O NMR spectra were recorded with an accumulation of ca. 680k scans, 41 ms acquisition time, 0.1 s relaxation delay, and 21 μs pulse length (π/2 flip angle). These experiments were conducted at 21 °C for ^{183}W, 27 °C for ^{51}V, and 55 °C for ^{17}O. Chemical shifts were referenced to external standards (δ = 0 ppm) that are 1 M Na_2WO_4 aqueous solution for ^{183}W, 90% $VOCl_3$ in C_6D_6 for ^{51}V, and H_2O for ^{17}O.

Infrared spectroscopy. Fourier Transform Infrared (FT-IR) spectra were recorded on a 6700 FT-IR Nicolet spectrophotometer, using diamond ATR technique. The spectra were recorded on non-diluted compounds in the range 400-4000 cm^{-1}. The IR spectra are provided in Supporting Information (See Figure S1).

UV-vis spectroscopy. UV-vis spectra of powdered compounds (see Figures S2 and S3) have been collected by using a Perkin-Elmer Lambda 750 spectrophotometer equipped with a powder sample holder set. The UV-vis spectra of solutions were recorded on a Perkin-Elmer Lambda-750 using calibrated 0.1 cm Quartz-cell.

Single-Crystal X-ray Diffraction. Crystals of compounds were selected under polarizing optical microscope and glued in paratone oil. X-ray intensity data were collected at low temperature (T = 220(2) K) on a Bruker D8 VENTURE diffractometer equipped with a PHOTON III C14 using a high brilliance IμS microfocus X-ray Mo Kα monochromatized radiation (λ = 0.71073 Å), except for compound $\mathbf{1}^{red}.\boldsymbol{C_{2v}}$ which was collected with a diffractometer equipped with a PHOTON 100. Data reduction was accomplished with SAINT V7.53a. The substantial redundancy in data allowed a semi-empirical absorption correction (SADABS V2.10) to be applied, on the basis of multiple measurements of equivalent reflections. Using Olex2,[49] the structure was solved with the ShelXT[50] structure solution program integrating Intrinsic Phasing and refined with the ShelXL[51] refinement package by Least Squares minimization. The remaining non-hydrogen atoms were located from Fourier differences and were refined with anisotropic thermal parameters. Crystallographic data for single-crystal X-ray diffraction studies are summarized in Table 1. These data can be obtained free of charge from The Cambridge Crystallographic Data Centre via

https://www.ccdc.cam.ac.k/structures-beta/. Deposit numbers: 2151664, 2151665, 2151666, 2151667 and 2151668 for $\mathbf{1}^{red}$**.**C_{2v}, $\mathbf{1}^{red}$**.**D_{3h}, $\mathbf{1}^{ox}$**.**D_{3h}, $\mathbf{2}^{red}$**.**D_{3h} and $\mathbf{2}^{ox}$**.**D_{3h}, respectively.

Table 1: Crystal data and structure refinement for $\mathbf{1}^{red}$.C_{2v}, $\mathbf{1}^{red}$.D_{3h}, $\mathbf{1}^{ox}$.D_{3h}, $\mathbf{2}^{red}$.D_{3h} and $\mathbf{2}^{ox}$.D_{3h}.

Compound	$\mathbf{1}^{red}$.C_{2v}	$\mathbf{1}^{red}$.D_{3h}	$\mathbf{1}^{ox}$.D_{3h}	$\mathbf{2}^{red}$.D_{3h}	$\mathbf{2}^{ox}$.D_{3h}
Empirical formula	$W_{18}V_3As_2Rb_{4.75}Na_6H_{33.25}O_{85}$	$W_{18}V_3As_2K_{10.5}H_{41.5}O_{89}$	$W_{18}V_3As_2K_9H_{32}O_{85}$	$W_{18}V_3Sb_2K_{10.5}H_{41.5}O_{89}$	$W_{18}V_3Sb_2K_9H_{32}O_{85}$
Formula weight	5549.15	5468.04	5355.87	5581.72	5449.55
Temperature/K	100(2)	220(2)	220(2)	220(2)	220(2)
Crystal system	Monoclinic	Triclinic	Monoclinic	Triclinic	Monoclinic
Space group	$P2_1/m$	P-1	$C2/m$	P-1	$C2/m$
a/Å	14.8853(10)	12.6076(6)	18.8433(6)	12.6417(4)	18.8242(7)
b/Å	19.0732(15)	18.1605(9)	16.9616(6)	18.1320(6)	16.9580(7)
c/Å	16.2430(13)	20.6707(9)	27.8746(10)	20.7217(6)	27.8624(10)
α/°	90	88.168(2)	90	88.172(2)	90
β/°	109.070(2)	86.951(2)	95.301(3)	86.928(2)	95.598(3)
γ/°	90	74.893(2)	90	74.727(2)	90
Volume/Å^3	4358.5(6)	4561.9(4)	8871.0(5)	4574.7(3)	8851.8(6)
Z	2	2	4	2	4
ρ_{calc}g/cm^3	4.209	4.078	3.960	4.152	4.048
μ/mm^{-1}	27.477	24.205	24.734	24.019	24.665
F(000)	4786	4942	9206	5008	9372
Crystal size/mm^3	0.22 × 0.12 ×0.10	0.28 × 0.18 × 0.1	0.18 × 0.12 × 0.08	0.2 × 0.15 × 0.1	0.18 × 0.11 × 0.05
Radiation	MoKα (λ = 0.71073)	MoKα (λ = 0.71073)	MoKα (λ = 0.71073)	MoKα (λ = 0.71073)	MoKα (λ = 0.71073)
2Θ range for data collection/°	3.598 to 50.288	3.948 to 50.058	3.47 to 50.07	4.538 to 50.21	3.644 to 50.198
Index ranges	$-17 \le h \le 17$ $-22 \le k \le 22$ $-19 \le l \le 19$	$-14 \le h \le 15$ $-21 \le k \le 21$ $-24 \le l \le 24$	$-22 \le h \le 22$ $-20 \le k \le 20$ $-33 \le l \le 33$	$-15 \le h \le 15$ $-21 \le k \le 21$ $-24 \le l \le 24$	$-22 \le h \le 22$ $-20 \le k \le 20$ $-33 \le l \le 33$
Reflections collected	195808	232876	179540	173747	199952
Independent reflections	8033 R_{int} = 0.0650 R_{sigma} = 0.0205	16103 R_{int} = 0.0667 R_{sigma} = 0.0275	8123 R_{int} = 0.0675 R_{sigma} = 0.0192	16186 R_{int} = 0.0668 R_{sigma} = 0.0342	8128 R_{int} = 0.0902 R_{sigma} = 0.0291
Data/restraints/parameters	8033/552/622	16103/36/1207	8123/12/591	16186/24/1225	8128/42/583
Goodness-of-fit on F^2	1.161	1.038	1.062	1.041	1.189
Final R indexes [I>=2σ (I)]	R_1 = 0.0599 wR_2 = 0.1319	R_1 = 0.0334 wR_2 = 0.1057	R_1 = 0.0324 wR_2 = 0.0931	R_1 = 0.0292 wR_2 = 0.0805	R_1 = 0.0358 wR_2 = 0.0989
Final R indexes [all data]	R_1 = 0.0687 wR_2 = 0.1382	R_1 = 0.0387 wR_2 = 0.1106	R_1 = 0.0385 wR_2 = 0.0986	R_1 = 0.0350 wR_2 = 0.0842	R_1 = 0.0393 wR_2 = 0.1068
Largest diff. peak/hole / e Å^{-3}	3.20/-2.72	3.20/-2.60	3.33/-1.99	3.45/-2.74	3.51/-2.28

RESULTS and DISCUSSION

Preparation of reduced and oxidized derivatives.

The previously published vanadyl containing $[(VO)_3(XW_9O_{33})_2]^{11/12-}$ with X = As^{III} and Sb^{III} have been obtained using different synthesis conditions (*p*H, temperature, reaction time, counter cations, VO^{2+}/$[\alpha\text{-B-}XW_9O_{33}]^{9-}$ ratio).[21–23] To elucidate the key synthetic parameters, we investigated their influences in buffered solutions (*p*H = 4.5) containing stoichiometric amount of vanadyl sulfate and $[\alpha\text{-B-}XW_9O_{33}]^{9-}$ unit. Our observations indicate the temperature and reaction time are crucial parameters providing the selective preparation of As^{III} based Hervé-type POMs with either a C_{2v} or a D_{3h} symmetry (see Figure 2). Using short reaction times (~15 minutes) at room temperature, the C_{2v} polyoxoanion $[(H_2O)(VO)_3(AsW_9O_{33})_2]^{12-}$ was isolated quantitatively by precipitation with RbCl. Recrystallisation in sodium chloride solution leads to reddish crystals formulated $H_{1.25}Rb_{4.75}Na_6[(H_2O)(VO)_3(AsW_9O_{33})_2]\cdot 15H_2O$ (notated $\mathbf{1^{red}}.\boldsymbol{C_{2v}}$). In contrast, heating the same reaction mixture at 70°C during 12 hours allows the preparation of polyoxoanion $[(VO)_3(AsW_9O_{33})_2]^{12-}$ with D_{3h} symmetry, that has been isolated as potassium salt $H_{1.5}K_{10.5}[(VO)_3(AsW_9O_{33})_2]\cdot 20H_2O$ (notated $\mathbf{1^{red}}.\boldsymbol{D_{3h}}$). Interestingly, when Sb^{III} is used as heteroelement, we systematically crystallized the Hervé-type POM $[(VO)_3(SbW_9O_{33})_2]^{12-}$ with D_{3h} symmetry (see Figure 2), formulated $H_{1.5}K_{10.5}[(VO)_3(SbW_9O_{33})_2]\cdot 20H_2O$ (notated $\mathbf{2^{red}}.\boldsymbol{D_{3h}}$).

Analysis of the synthetic procedures reported by Mialane et *al.*[21] or Krebs et *al.*[19] supports our observations. Short heating period (15 min at 50 °C) of the synthetic mixture leads to the co-crystallization of C_{2v} and D_{3h} anions while a two-weeks period before crystallization gave exclusively the D_{3h} anion $[(VO)_3(AsW_9O_{33})_2]^{12-}$. Besides, the use of Sb^{III}-containing derivative affords only the formation of Hervé-type POMs with a D_{3h} symmetry in accordance with the previous report of Yamase and coworkers.[20]

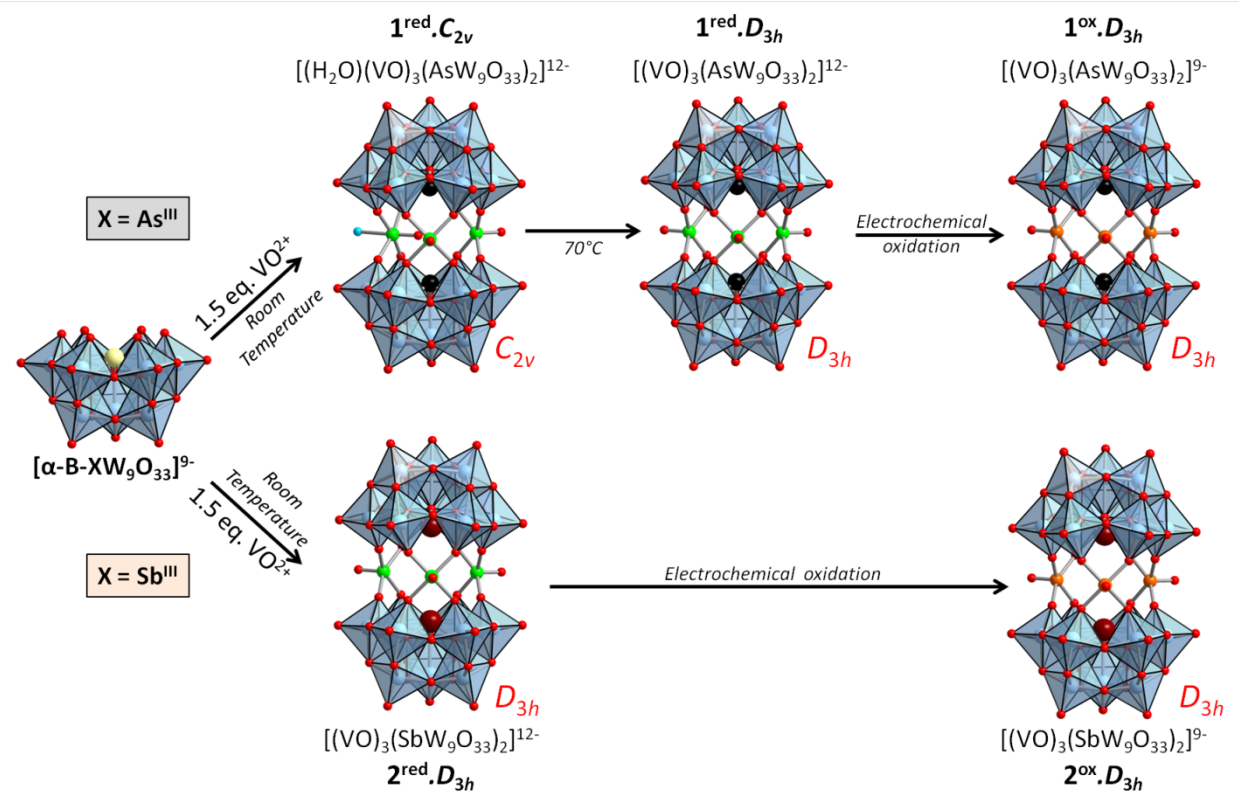

Figure 2: Schematic illustration showing the synthetic pathways allowing the preparation of the vanadium-containing Hervé-type POMs built from B-type trivacant Keggin derivatives $[XW_9O_{33}]^{9-}$. Color code: cyan octahedra: WO_6; green sphere: V^{4+}; orange sphere: V^{4+}; turquoise sphere: aquo group; black sphere: As; brown sphere: Sb.

Then, the oxidized forms of D_{3h} species were obtained by electrochemical oxidation using controlled potential with a carbon electrode polarized at 0.6 V vs Ag/AgCl, from solutions of as-synthesized reduced anions $[(VO)_3(XW_9O_{33})_2]^{12-}$ (12 mM of POM in acetate buffer, *p*H = 4.5). Electrolysis progress was followed by UV-vis spectroscopy highlighting the decrease of two absorption bands located at ~520 and ~760 nm, corresponding to the intervalence charge transfer transitions ($V^{IV} \rightarrow W^{VI}$ IVCT) and d-d transitions of V^{IV}, respectively. As an illustrative example, the electrochemically controlled oxidation of the $\mathbf{1^{red}}.\boldsymbol{D_{3h}}$ is presented in Figure 1. These absorptions decrease linearly as featured by the variation of the average molar absorption coefficients from $\bar{\varepsilon}_{520} \sim 1000$ $M^{-1}cm^{-1}$ and $\bar{\varepsilon}_{760} = 450$ $M^{-1}cm^{-1}$ to 0 until the full oxidation of the three V^{IV} into V^{V} ions which is consistent with complete process for 3 F/mol charge consumption (see Figure 3). Besides, it is worth to note the wavelength range for the $V^{IV} \rightarrow W^{VI}$ IVCT is similar to that observed for the mixed $[XW_{11}VO_{40}]$ Keggin-type anions (with X = P, Si, B, Zn, H_2).[52] As

expected, the oxidized form exhibits a more intense absorption at 370 nm ($\bar{\varepsilon}_{370}$ = 14400 $M^{-1}cm^{-1}$) than the reduced derivative ($\bar{\varepsilon}_{370}$ = 1800 $M^{-1}cm^{-1}$) (see Figure S2). After completed oxidation process, a yellowish solid $K_9[(VO)_3(AsW_9O_{33})_2]\cdot 16H_2O$ (**1**^{ox}***D*$_{3h}$) was precipitated with KCl. Suitable single-crystals of **1**^{ox}***D*$_{3h}$ were obtained after recrystallization in water. Similar procedure was also applied to isolate the oxidized Sb^{III}-based form (notated hereafter **2**^{ox}***D*$_{3h}$), giving a crystalline solid $K_9[(VO)_3(SbW_9O_{33})_2]\cdot 16H_2O$. The evolution of the electronic spectra of the Sb^{III} derivative during the oxidation is similar to that observed for the As^{III} containing POM (see Figure S3). It must be mentioned the oxidation of **1**^{red}***C*$_{2v}$ leads to a mixture of oxidized C_{2v} and D_{3h} species, highlighting that fraction of the kinetic C_{2v} polyoxoanion converts into the thermodynamic D_{3h} product in the course of the oxidative electrolysis process.

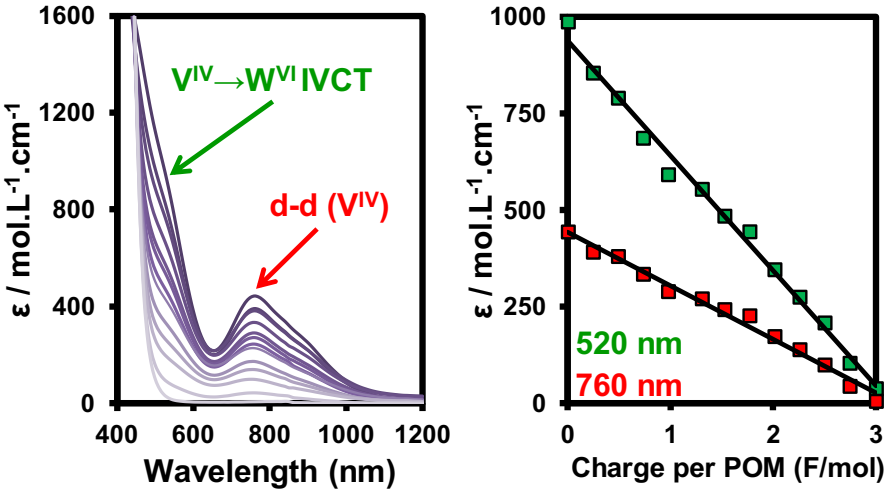

Figure 3: UV-vis spectra of $[(VO)_3(AsW_9O_{33})_2]^{12-}$ during electrochemical oxidation, showing the decreases of the characteristic absorption bands related to $V^{IV}\rightarrow W^{VI}$ IVCT (λ = 520 nm) and d-d transitions of V^{IV} (λ = 760 nm). The average molar absorption coefficients of characteristic bands of $[(VO)_3(AsW_9O_{33})_2]^{12-}$ decrease linearly with the oxidation of the vanadium centers.

Comparison of the crystal structures.

The potassium salts of the D_{3h} polyanions $[(VO)_3(XW_9O_{33})_2]^{12-}$ with X = As (**1**^{red}***D*$_{3h}$) or Sb (**2**^{red}***D*$_{3h}$) crystallize both in triclinic system (volume ~ 4567 ± 10 Å^3; space group: *P*-1). It must be mentioned the C_{2v} polyoxoanion $[(H_2O)(VO)_3(AsW_9O_{33})_2]^{12-}$ isolated as potassium salt also crystallizes with unit cell parameters similar to those observed for **1**^{red}***D*$_{3h}$ and **2**^{red}***D*$_{3h}$, however the crystals were not suitable for structure elucidation. Therefore, the C_{2v} polyoxoanion $[(H_2O)(VO)_3(AsW_9O_{33})_2]^{12-}$ has been isolated as mixed sodium/rubidium salt (compound **1**^{red}***C*$_{2v}$), and the X-ray diffraction data analysis was consistent with a monoclinic system (volume ~ 4358

Å^3; space group: $P2_1/m$). Crystals of oxidized polyoxoanions $[(VO)_3(XW_9O_{33})_2]^{9-}$ as potassium salt with X = As (**1**^{ox}***D***$_{3h}$) or Sb (**2**^{ox}***D***$_{3h}$) exhibit also similar unit cells (volume ~ 8861 ± 10 Å^3; space group: $C2/m$). In all crystal structures, the polyanion is built from two $[\alpha\text{-B-}XW_9O_{33}]^{9-}$ anionic units linked together by three vanadium centers forming a triangle (see Figure 4).

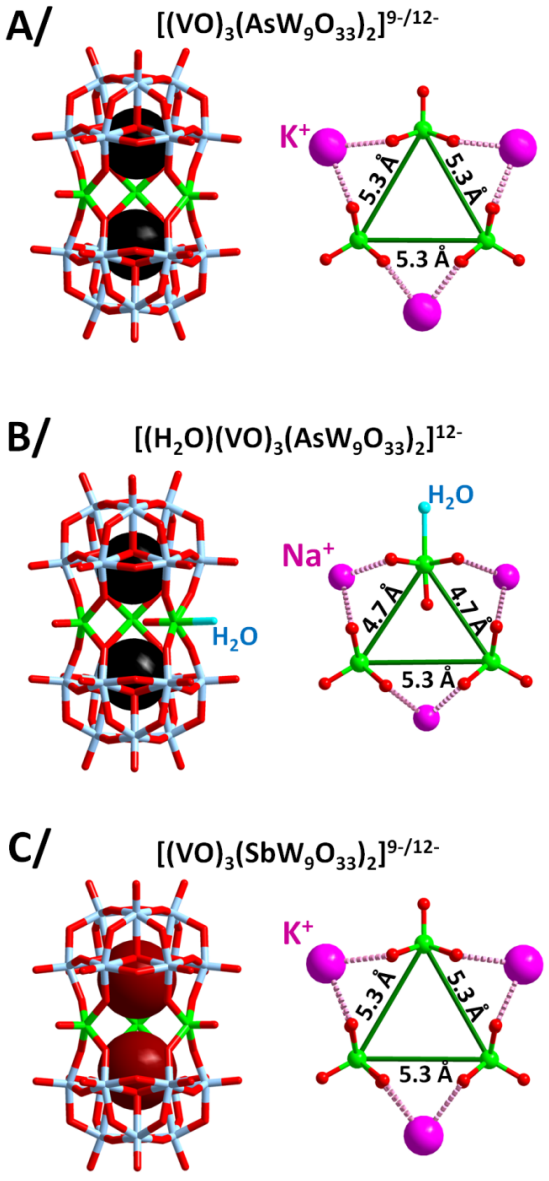

Figure 4: Structural models of the D_{3h} polyoxoanions $[(VO)_3(AsW_9O_{33})_2]^{9-/12-}$ (A), the C_{2v} polyoxoanion $[(H_2O)(VO)_3(AsW_9O_{33})_2]^{12-}$ (B) and the D_{3h} polyoxoanions $[(VO)_3(SbW_9O_{33})_2]^{9-/12-}$ (C), showing the size of the cavity located between the Keggin-type fragments is larger for the As^{III} based POM than for Sb^{III} one. Within the vanadium triangle, the V-V distances is affected by the symmetry of the metal-oxo frameworks (C_{2v} or D_{3h}). The heteroatoms have been represented in space-filling. Color code: cyan: W; red: O of oxo group, turquoise: O of aquo group; pink: alkali cations (Na^+ or K^+), green: V; black sphere: As and brown sphere: Sb.

In the D_{3h} arrangements, noted $\mathbf{1}^{red}$.$\boldsymbol{D_{3h}}$, $\mathbf{1}^{ox}$.$\boldsymbol{D_{3h}}$, $\mathbf{2}^{red}$.$\boldsymbol{D_{3h}}$ and $\mathbf{2}^{ox}$.$\boldsymbol{D_{3h}}$, all vanadium centers adopt exclusively the typical square pyramidal environment VO_5, wherein their V=O bond appears outward directed that results of the high D_{3h} symmetry. Additionally, three potassium ions are located in sites alternating with vanadium atoms and are bound to four oxygen atoms of the W-O-V bridges (see Figures 4A and 4C). The structural analysis of the oxidized and reduced D_{3h} species reveals that bond distances and angles remains quite similar within the $\{XW_9O_{33}\}$ subunits but differ significantly in the vicinity of the vanadium centers in relationship with the +V or +IV oxidation state. Bond lengths of the terminal {V=O} and those of the {V-O-W} bridges are reported in Table 2. While the V=O bond lengths remain almost unchanged for all compounds, the V-O bond distances are shortened by about 0.09 Å for the oxidized compounds. This is a direct consequence of the presence of V^V centers. Concomitantly to the shrinkage of the V-O bonds, a slightly lengthening of the W-O bond within the {V-O-W} bridges is observed (+ 0.05 Å).

In the C_{2v} polyoxoanion $[(H_2O)(VO)_3(AsW_9O_{33})_2]^{12-}$ ($\mathbf{1}^{red}$.$\boldsymbol{C_{2v}}$), the structural arrangement is similar to the D_{3h} polyanion $[(VO)_3(AsW_9O_{33})_2]^{12-}$ except the vanadium-based triangle linking the two $\{AsW_9\}$ units (see Figure 4B). In the C_{2v} arrangement, the three vanadium centers form an isosceles triangle with two short sides (V···V = 4.7 Å) and one longer (V···V = 5.3 Å). This distortion is due to the presence of a six-fold coordinated vanadium center adopting a pseudo octahedral environment. The {V=O} group of this vanadium center is directed toward the inner cavity of POMs (see Figure 4B), while the two other vanadium centers point toward the exterior as observed in the D_{3h} POM. Furthermore, the coordination shell of the six-fold coordinated vanadium is completed by a binding water molecule (d_{V-O} = 2.27(2) Å). Three sodium ions are located in sites alternating with vanadium atoms (see Figure 4B).

X-ray diffraction studies and previous reported results highlight the possibility to incorporate an oxygen atom within the inner cavity delimited by the two As^{III} through the 180° rotation of one {V=O} group. Actually, the size of the inner space should be strongly affected by the nature of the two heteroatoms X. As showed in Figure 4, this space appears quite cancelled when the ionic radius of the X^{3+} ion increases from 1.85 Å (for X = As) to 2.05 Å (for X = Sb). Furthermore, electrostatic repulsions between the lone pair of the X^{III} atoms and the inner oxygen atom must be also considered. Finally, steric hindrance and unfavorable electrostatic interactions are probably large enough within the Sb-containing derivative to prevent the formation of the C_{2v} species.

Conversely, as the size of the heteroatom is reduced, the resulting increase of the inner space offers the possibility to contain one oxygen atom of one {V=O} moiety, leading to the formation of the C_{2v} arrangement.

Table 2: Bond lengths and bond valence sums of the reduced (V^{IV}-containing) and oxidized (V^{V}-containing) polyoxoanions. The bond valence calculations have been performed according to the B and R_0 parameters defined by Brown and Altermatt.[53]

Compounds	**1^{red}.D_{3h}**	**2^{red}.D_{3h}**	**1^{ox}.D_{3h}**	**2^{ox}.D_{3h}**	**1^{red}.C_{2v}**	
Environment	square pyramidal	square pyramidal	square pyramidal	square pyramidal	square pyramidal	octahedral
V=O (Å)	1.582(7) - 1.605(7)	1.591(7) - 1.604(6)	1.587(9) - 1.59(1)	1.57(1) - 1.58(1)	1.62(2)	1.61(3)
V-O^{oxo} (Å)	1.943(7) - 1.980(6)	1.948(6) - 1.991(7)	1.863(8) - 1.886(8)	1.863(8) - 1.882(9)	1.95(2) - 1.97(2)	1.88(2) - 1.94(2)
V-O^{H2O} (Å)	-	-	-	-	-	2.27(2)
W-O (Å)	1.798(6) - 1.825(7)	1.808(7) - 1.839(7)	1.863(8) - 1.880(8)	1.876(8) - 1.891(8)	1.80(1) - 1.83(1)	
Average BVS[a] of the V centers	4.16	4.13	5.15	5.15	4.22	

[a] For BVS calculations: B = 0.37; R_0 = 1.804 (V^{5+}) or 1.784 (V^{4+}).

Multinuclear NMR characterization of the oxidized derivatives.

^{17}O, ^{51}V and ^{183}W NMR spectra of the oxidized D_{3h} Hervé-type POMs $[(VO)_3(XW_9O_{33})_2]^{9-}$ with X = As^{III} or Sb^{III} recorded in aqueous solution are fully consistent with the presence of the D_{3h} polyoxoanions (see Figure 5).

The ^{183}W NMR spectrum of D_{3h} Hervé-type POM $[(VO)_3(AsW_9O_{33})_2]^{9-}$ as potassium salt (**1^{ox}.D_{3h}** dissolved in D_2O) revealed two resonance lines. These two signals, located at -99.2 and -128.3 ppm with a signal area ratio of 2:1 and should be assigned to the six-W belt and to the three-W cap of the D_{3h} polyanion, respectively. Furthermore, the three-W cap resonance appears quite narrow ($\Delta\nu_{1/2}$ < 2 Hz) while the signal of the six-W belt exhibits a significant broadening ($\Delta\nu_{1/2}$ = 28 Hz) due to their proximity to the ^{51}V quadrupolar nucleus (I = 7/2). The ^{51}V NMR spectrum exhibits only one signal located at -541 ppm. The ^{51}V NMR spectrum of freshly dissolved $[(VO)_3(SbW_9O_{33})_2]^{9-}$ as potassium salt (powder of **2^{ox}.D_{3h}** dissolved in D_2O) shows only one single peak located at -532 ppm, while the ^{183}W NMR spectrum exhibits two signals located at -89.8 ($\Delta\nu_{1/2}$ = 25 Hz) and -118.2 ppm ($\Delta\nu_{1/2}$ < 2 Hz) with intensity ratio 2:1 corresponding respectively

to the six-W belt and three-W cap of the two equivalent {α-B-SbW_9O_{33}} subunits. We note the low-field shift of both ^{183}W and ^{51}V NMR signals in $[(VO)_3(SbW_9O_{33})_2]^{9-}$ when compared to $[(VO)_3(AsW_9O_{33})_2]^{9-}$ by about 10 ppm. Such magnetic shielding is a typical effect of heavier Sb nucleus by comparison to As.[33,54]

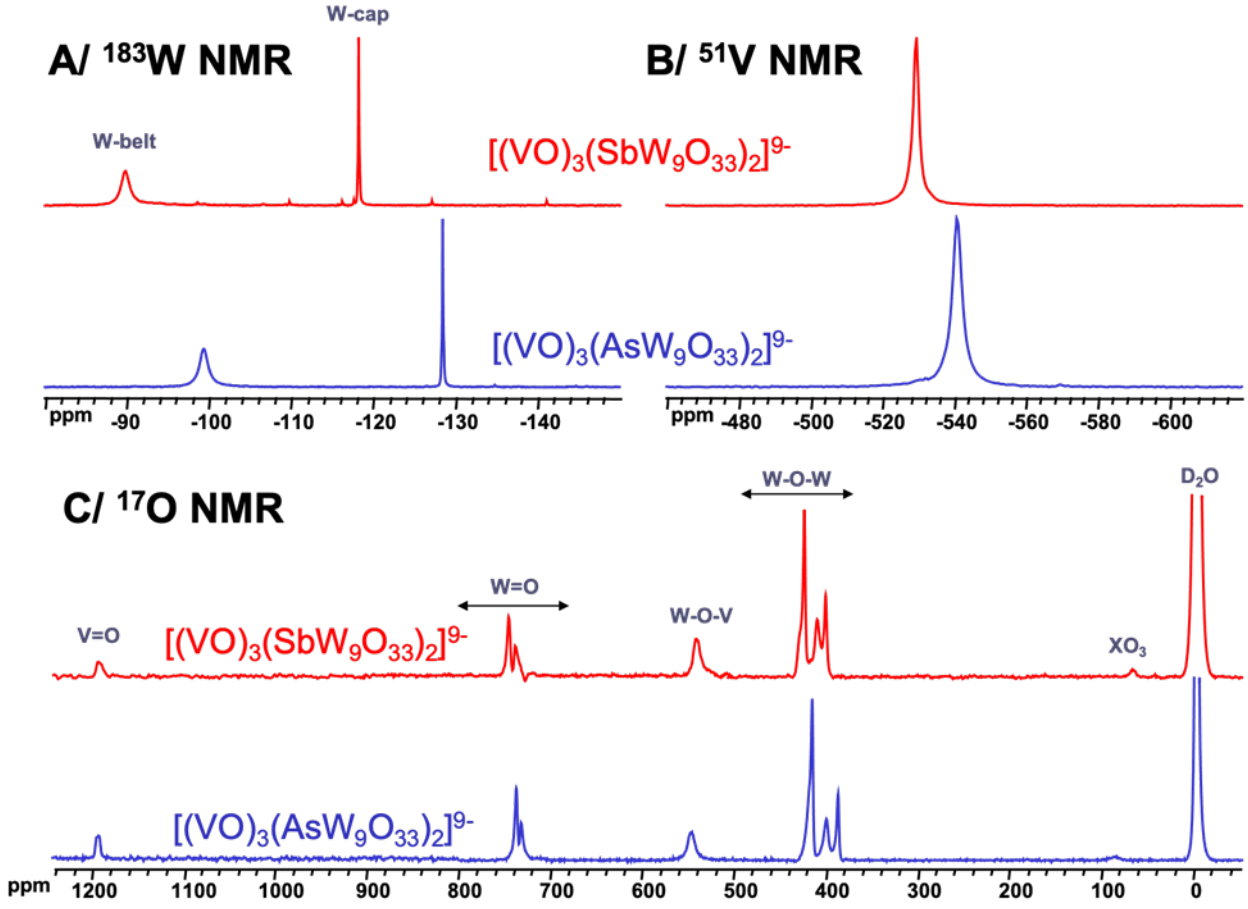

Figure 5. ^{183}W (A), ^{51}V (B), and ^{17}O (C) NMR spectra of the D_{3h} polyanions $[(VO)_3(AsW_9O_{33})_2]^{9-}$ (blue spectra) and $[(VO)_3(AsW_9O_{33})_2]^{9-}$ (red spectra) in aqueous solution.

^{17}O NMR provides further structural information in relationship to the diversity of O sites in POMs. The aqueous solution of the D_{3h} $[(VO)_3(XW_9O_{33})_2]^{9-}$ anion gives ^{17}O NMR spectrum showing nine lines with the expected 2:2:2:4:2:4:2:4:1 intensity ratio. The chemical shift and linewidth data are listed in Table 3. We note the strong shielding effect on the resonances corresponding to the terminal and bridging oxygen atoms linked to vanadium by comparison to those attributed to {W-O} groups.[55] Furthermore, the $\{XO_3\}$ resonance appear quite sensitive to the nature of heteroatom X leading to a significant deshielding effect at the ^{17}O nuclei when As is substituted for Sb atom.

Besides, the remaining ^{17}O resonances appear rather few affected through the nature of X and undergo variations less than 10 ppm (see Table 3). Such effects, although small, should translate the slight variations of bond distances and angles when As is changed by the bulkier Sb heteroatom in the {α-B-XW_9O_{33}} subunits.

Table 3: NMR data of D_{3h} polyanion of $[(VO)_3(XW_9O_{33})_2]^{9-}$, X = As^{III} and Sb^{III}.

	Multiplicity	**X = As** δ / ppm ($\Delta\nu_{1/2}$ / Hz)	**X = Sb** δ / ppm ($\Delta\nu_{1/2}$ / Hz)
^{51}V site			
V=O	1	-541 (350)	-532 (390)
^{183}W sites			
W-cap	1	-128.3 (2)	-118.2 (2)
W-belt	2	-99.2 (28)	-89.8 (25)
^{17}O sites			
XO_3	2	88.4 (640)	67.3 (540)
W-O-W	2	387.7 (160)	395.7 (140)
	2	400.1 (320)	405.3 (130)
	4	415.5 (110)	418.1 (120)
	2	418.6 (320)	424.0 (180)
W-O-V	4	546.7 (560)	537.7 (380)
W=O	2	731.3 (220)	735.3 (140)
	4	737.4 (200)	742.3 (200)
V=O	1	1199.4 (290)	1199.3 (260)

The ^{51}V and ^{183}W NMR investigations of the freshly oxidized solution of **1^{red}.C_{2v}** clearly indicate the coexistence of two species. The ^{183}W NMR spectrum (see Figure S4) is featured by four minor signals, and two main resonance lines that correspond to D_{3h} Hervé-type POM $[(VO)_3(AsW_9O_{33})_2]^{9-}$. For the oxidized C_{2v} polyanion $[(H_2O)(VO)_3(AsW_9O_{33})_2]^{9-}$, we expectfive peaks with relative intensity of 1:2:2:2:2. The four minor signals have been observed at -90.9 ($\Delta\nu_{1/2}$ = 19 Hz), -126.4 ($\Delta\nu_{1/2}$ = 19 Hz), -134.7 ($\Delta\nu_{1/2}$ = 5 Hz) and -144.6 ppm ($\Delta\nu_{1/2}$ = 5 Hz) with intensity ratio close to 2:2:2:1 (6% / 4% / 7% / 3%), respectively. These signals should be consistent with the presence of the C_{2v} polyanion, although one additional broad peak integrating for 2 is missing, probably due to an accidental degeneracy with the broad -99.2 ppm signal of the six-W belt from the D_{3h} arrangement. Such hypothesis could be supported by the slight overestimation of its intensity (+5%) with respect to the expected value from the intensity of the three-W cap of the D_{3h} polyanion. Actually, proportion of the two POMs can be estimated on the basis of our hypothesis, leading to 70% for the D_{3h} species and 30% for the other C_{2v} anion. While three ^{51}V resonances are expected for mixture of both isomers, the presence of two peaks located at -541 and -530 ppm is

probably due to still an accidental overlapping. As expected, the conversion process of the C_{2v} species into D_{3h} polyanion $[(VO)_3(AsW_9O_{33})_2]^{9-}$ is accelerated by the heating. After heating 90 °C during 5 h, a single ^{51}V resonance located at -541 ppm is observed (see Figure S4). In a similar way, the ^{183}W NMR spectrum of the heated solution revealed also a pure solution of D_{3h} polyanion $[(VO)_3(AsW_9O_{33})_2]^{9-}$ (see Figure S4). Supported by structural X-ray analyses and NMR studies, we have show that the C_{2v} polyanion $[(H_2O)(VO)_3(AsW_9O_{33})_2]^{9/12-}$ is thermodynamically unstable and can be selectively converted into the D_{3h} anions. A possible explanation of the thermodynamic instability of the C_{2v} polyanion is that water molecule linked to one vanadium center, produced locally a structuration of the solvent water molecules. This induces an energy cost that can be eliminated by reversal the V=O bond pointed initially toward the cavity. This process leads to the D_{3h} polyanion exhibiting exclusively terminal oxo groups exposed to the solvent.

Hydrolytic stability of the D_{3h} oxidized derivatives. The stability of the oxidized D_{3h} forms $[(VO)_3(XW_9O_{33})_2]^{9-}$ with X = As^{III} and Sb^{III} have been studied in aqueous solution by ^{51}V NMR in the *p*H range 0 to 9.5 (Figure S5). For both compounds, the ^{51}V NMR features do not change for *p*H values between 1 and 6. A continuous downfield shift of the ^{51}V NMR signal is however observed for the *p*H values below 1, indicating the protonation of the POM units in such conditions (see Figure S6). Actually, these results indicate the fair stability of the oxidized POMs in acidic medium. Nevertheless, the $[(VO)_3(SbW_9O_{33})_2]^{9-}$ anion starts to decompose at about *p*H = 6.3 and disappear completely above *p*H = 6.8 (Figure S5). On the other hand, $[(VO)_3(AsW_9O_{33})_2]^{9-}$ species can still persist at *p*H 8.4 and decomposition only begins at *p*H = 7.3. In this *p*H range, the narrow ^{51}V NMR signal located at -509 ppm is consistent with the presence of mixed-metal Lindqvist anion *cis*-$[W_4V_2O_{19}]^{4-}$,[18,56] which corresponds to the single vanadium-containing decomposition product. Furthermore, such a study suggests that the As derivative is more robust than the Sb derivative toward basic degradation.

Electrochemical behavior. The cyclic voltammograms (CVs) of the D_{3h} derivatives have been measured in sulfate electrolytes (0.5 M) with *p*H values varying from about 0.3 to 6. Besides, the investigations revealed that the oxidized $[(VO)_3(XW_9O_{33})_2]^{9-}$ or reduced $[(VO)_3(XW_9O_{33})_2]^{12-}$ species exhibit perfectly superimposed CVs. Furthermore, electrochemical features do not allow discriminating between the As^{III} and the Sb^{III} derivatives (see Figure S7 for electrochemical data of Sb^{III} derivative), both leading to comparable electrochemical behavior in the 0-6 *p*H range. Then,

only the electrochemical behavior of the As^{III} derivative $[(VO)_3(AsW_9O_{33})_2]^{9-}$ (**1^{ox}.*D*$_{3h}$**) is described hereafter in details.

CVs of $[(VO)_3(AsW_9O_{33})_2]^{9-}$ shown in Figure 6a reveals that electrochemical behavior is strongly dependent upon *p*H. Besides, it should be worth mentioning that current variations of the anodic and cathodic peak exhibit both a linear dependence upon square root of the potential scan rate, indicating a diffusion-controlled electron-transfer kinetic (see Figure S8). At *p*H = 0.3, the CV pattern is consistent with a quasi-reversible 3-electron redox wave (V^{V}_3/V^{IV}_3) which corresponds to the simultaneous three one-electron transfers involving the three equivalent vanadium centers. The apparent $E_{1/2}$ of this redox wave is observed at +0.49 V *vs* Ag/AgCl. Coulometric studies, supported by UV-vis spectrometry have confirmed that this electrochemical event involves three electrons (see Figure S9). Interestingly, this 3-electron transfer appears altered significantly with *p*H. As shown in Figure 6, *p*H increasing provokes the concomitant monotone decrease of the apparent $E_{1/2}$ potential and the gradual splitting of the three-electron transfer into three successive monoelectronic events identified at + 0.47, +0.39 and +0.27 V *vs* Ag-AgCl (see Figures 6a and 6b). Splitting of the 3-electron wave becomes visible at *p*H = 1.5. At *p*H = 2, two distinct redox waves are distinguished, corresponding to a mono-electronic and a bi-electronic redox transfer located at +0.47 and +0.39 V *vs* Ag/AgCl, respectively. Increasing *p*H further induces the complete splitting of the bi-electronic redox event. At *p*H = 4.5, three quasi-reversible and successive mono-electronic redox waves are observed clearly at +0.47, +0.39 and +0.27 V *vs* Ag/AgCl. For higher *p*H up to 6, the CV remains almost unchanged and corresponds to that reported by Yamase et al. as preliminary electrochemical study of the reduced $[(VO)_3(SbW_9O_{33})_2]^{12-}$ anion.[23]

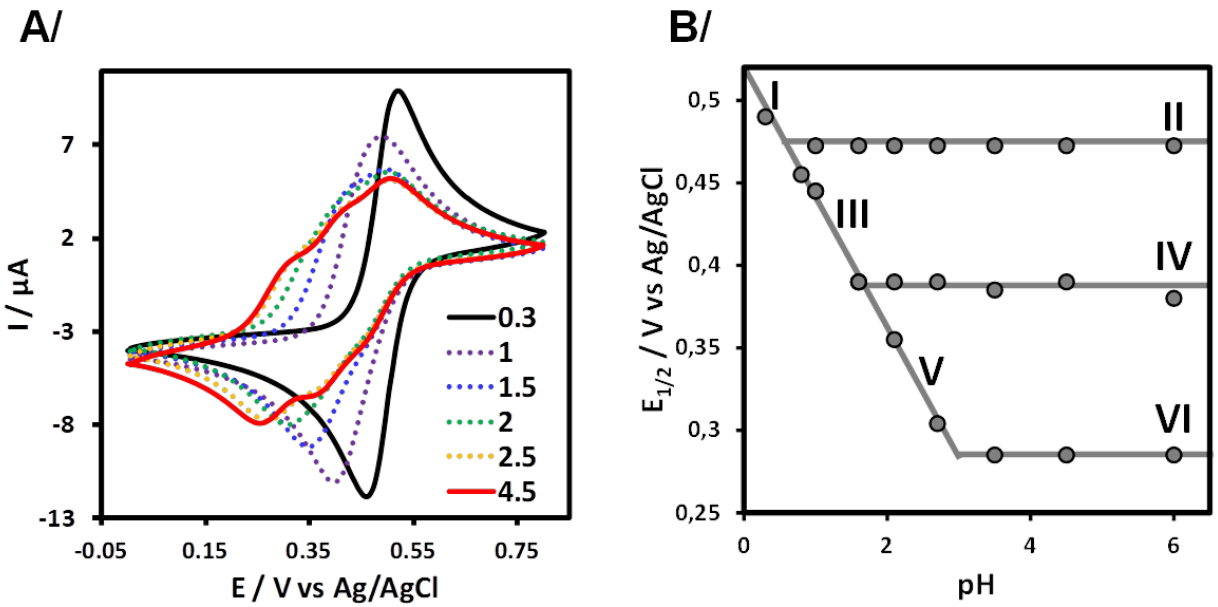

Figure 6. a) Cyclic voltammograms of 2 mM solutions of $[(VO)_3(AsW_9O_{33})_2]^{9-}$ at different *p*H (from 0.3 to 4.5). Scan rate: 10 mV/s; b) Variation of apparent potentials of the different redox events as a function of acidity. Experimental points are represented by circles. The six different redox processes identified are labeled by roman numbers. The *p*H-dependency of the redox events I, III and V is about -65 mV/*p*H unit.

In summary, the electrochemical behavior of the oxidized compounds $[(VO)_3(AsW_9O_{33})_2]^{9-}$ (noted $\{V^V_3\}^{9-}$) is strongly altered over the 0 - 4.5 *p*H range, as shown by the potential-*p*H diagrammatic representation given in Figure 6b. The diagram delimits six domains numbered from I to VI (see Figure 6b). The redox domains labeled I, III and IV correspond to three *p*H-dependent redox processes which involves a trielectronic, a bielectronic and a monoelectronic process, respectively. The average slope of ~ -65 mV/*p*H unit is close to the theoretical value (- 59 mV/unit *p*H) expected for a simultaneous exchange of equal number of electrons and protons. Conversely, the domains labeled II, IV, VI correspond to three *p*H-independent monoelectronic redox couples. Then, these domains I-VI are representative of six redox events given in Table 4.

Table 4: Redox couples, related equations and potentials (V *vs* Ag/AgCl) illustrating the redox behavior of the sandwich-type anion $[(VO)_3(AsW_9O_{33})_2]^{9-}$ (**1^{ox}.*D*$_{3h}$**) over the 0-6 *p*H range.

Domain	*p*H range	Redox couple	Redox equation	$E_{1/2}$ (*p*H = 0)
I	*p*H < 0.8	$\{V^V_3\}/\{H_3V^{IV}_3\}$	$\{V^V_3\}^{9-} + 3\ e^- + 3\ H^+ \rightarrow \{H_3V^{IV}_3\}^{9-}$	+0.52
II	*p*H > 0.8	$\{V^V_3\}/\{V^V_2V^{IV}\}$	$\{V^V_3\}^{9-} + 1\ e^- \rightarrow \{V^{IV}_1V^V_2\}^{10-}$	+0.47

III	0.8 – 1.6	$\{V^{V}_{2}V^{IV}\}/\{H_2V^{IV}_{3}\}$	$\{V^{IV}_{1}V^{V}_{2}\}^{10-} + 2\ e^- + 2\ H^+ \rightarrow \{H_2V^{IV}_{3}\}^{10-}$	+0.52
IV	*p*H > 1.6	$\{V^{V}_{2}V^{IV}_{1}\}/\{V^{V}_{1}V^{IV}_{2}\}$	$\{V^{V}_{2}V^{IV}_{1}\}^{10-} + 1\ e^- \rightarrow \{V^{V}_{1}V^{IV}_{2}\}^{11-}$	+0.39
V	1.6 - 3	$\{V^{V}_{1}V^{IV}_{2}\}/\{HV^{IV}_{3}\}$	$\{V^{V}_{1}V^{IV}_{2}\}^{11-} + 1\ e^- + H^+ \rightarrow \{HV^{IV}_{3}\}^{11-}$	+0.52
VI	*p*H > 3	$\{V^{V}_{1}V^{IV}_{2}\}/\{V^{IV}_{3}\}$	$\{V^{V}_{1}V^{IV}_{2}\}^{11-} + 1\ e^- \rightarrow \{V^{IV}_{3}\}^{12-}$	+0.27

Furthermore, this electrochemical study allows estimating the pKa values of the 3-electron reduced form $[(VO)_3(AsW_9O_{33})_2]^{12-}$ which three weak acidities at pKa_1 ~0.8, pKa_2 ~1.5 and pKa_3 ~3). It is worth to note that the evolution of the electronic spectra of the $[(VO)_3(AsW_9O_{33})_2]^{12-}$ as a function of the *p*H (see Figure S10) shows a blue shift of the absorption maximum wavelength associated to the *d-d* transitions of the vanadyl centers when the *p*H decreases from ~3 to ~0.7. This observation is in good agreement with the electrochemical conclusions concerning the weak acidic properties of the reduced D_{3h} polyanion $[(VO)_3(AsW_9O_{33})_2]^{12-}$.

Cyclic voltammograms (CVs) of the C_{2v} polyanion $[(H_2O)(VO)_3(AsW_9O_{33})_2]^{12-}$ has been measured at *p*H = 0.3 and 4.5 in similar conditions to those used for the analysis of C_{2v} polyanion $[(H_2O)(VO)_3(AsW_9O_{33})_2]^{12-}$. The comparison of the CVs (see Figure S11), revealed the redox properties of the C_{2v} polyanion does not differ significantly to those of D_{3h} polyanion $[(VO)_3(AsW_9O_{33})_2]^{12-}$. Nevertheless, the redox event appears much less defined especially for *p*H = 4.5, suggesting not fully reversible redox process. This is probably due to the presence of one V=O bond directed toward the center of the cavity that change the geometry of the three V-centers from square pyramidal to octahedral. This terminal oxygen atom certainly induces a steric hindrance that limit the shrinkage of the V-O bonds during the oxidation of the V centers. As a consequence of this lack of reversibility, a part of the C_{2v} polyanion can be converted into the D_{3h} polyanion in which no oxygen atoms are in the central cavity. This hypothesis is confirmed by our multinuclear NMR studies that have revealed that the oxidized solution of $\mathbf{1^{red}}.\boldsymbol{C_{2v}}$ consists of a mixture of D_{3h} (70%) and C_{2v} (30%) species.

CONCLUSIONS

This revisited study of the archetypical sandwich-type compound $[(VO)_3(XW_9O_{33})_2]^{12-}$ firstly described by Yamase *et al*. (X= Sb)[23] or Mialane *et al*. (X = As)[21] provides further insights about structural and electrochemical features relevant with regard to potential applications in biology, catalysis or materials science. This report evidences that the fully oxidized vanadium (V) containing polyoxometalates $[(VO)_3(XW_9O_{33})_2]^{9-}$ with X = As^{III} or Sb^{III} can be prepared by

selective electrochemical oxidation of the fully reduced D_{3h} species $[(VO)_3(XW_9O_{33})_2]^{12-}$. Interestingly, such an electrochemical process consists of the oxidation of the three vanadyl centers, from V(IV) into V(V) which proceeds with a complete retention of the geometry of the vanadium centers. Besides, we evidenced the C_{2v} polyanion $[(H_2O)(VO)_3(AsW_9O_{33})_2]^{9/12-}$ is thermodynamically unstable and can be selectively converted into the D_{3h} anion. The structural characterization of the reduced and oxidized species showed that the square pyramidal geometry of the three vanadium centers is retained while a significant shrinkage of the coordination sphere is observed as V(IV) ions are converted into V(V). Then, full evidence of the interconversion process between the two redox states prompted us to investigate further electrochemical properties of D_{3h} polyanions. Actually, such a study revealed that redox properties of the $[(VO)_3(XW_9O_{33})_2]^{9-}$ anions are strongly altered within [0 - 6] *p*H range. In acidic conditions (*p*H < 0.8), POM exhibits a single quasi-reversible wave corresponding to a $3e^-/3H^+$ proton-coupled-electron-transfer (PCET). Such a transfer proceeds quasi-simultaneously because the vanadium centers are physically far from each other (V···V = 5.3 Å), thus minimizing electrostatic effects that are fully cancelled through the concomitant proton-coupled transfer process. Such electrostatic effects become observable at higher *p*H wherein the net transfer of three electrons occurs successively within a narrow potential range. Multi-PCET are ubiquitous in energy conversion or storage reactions suggesting that such sandwich-type POMs $\{(VO)_3(XW_9O_{33})_2\}$ could be used as (electro)catalyst or as electrons reservoir for applications in relationship with societal challenges.

ASSOCIATED CONTENT

Supporting Information. CIF files, Infrared spectra, UV-vis spectra, multinuclear NMR (*p*H stability), CVs of the Sb^{III} D_{3h} and the As^{III} C_{2v} derivatives.

The following files are available free of charge.

AUTHOR INFORMATION

Corresponding Author

* clement.falaise@uvsq.fr ; * emmanuel.cadot@uvsq.fr

Author Contributions

The manuscript was written through contributions of all authors. All authors have given approval to the final version of the manuscript.

ACKNOWLEDGMENT

Authors gratefully acknowledge financial support from LabEx CHARMMMAT (grant number ANR-11-LBX-0039). This work was also supported by i) University of Versailles Saint Quentin, ii) CNRS, iii) Région Ile de France through DIM Nano K and DIM Respore. I. Bamba thanks the Embassy of Ivory Coast in France for his scholarship.

REFERENCES

(1) Pope, M. *Heteropoly and Isopoly Oxometalates*; Inorganic Chemistry Concepts; Springer-Verlag: Berlin Heidelberg, 1983.

(2) Gumerova, N. I.; Rompel, A. Synthesis, Structures and Applications of Electron-Rich Polyoxometalates. *Nat. Rev. Chem.* **2018**, *2* (2), 1–20.

(3) N. Miras, H.; Yan, J.; Long, D.-L.; Cronin, L. Engineering Polyoxometalates with Emergent Properties. *Chem. Soc. Rev.* **2012**, *41* (22), 7403–7430.

(4) Anjass, M.; Lowe, G. A.; Streb, C. Molecular Vanadium Oxides for Energy Conversion and Energy Storage: Current Trends and Emerging Opportunities. *Angew. Chem. Int. Ed.* **2021**, *60*, 7522.

(5) Chen, J.-J.; Ye, J.-C.; Zhang, X.-G.; Symes, M. D.; Fan, S.-C.; Long, D.-L.; Zheng, M.-S.; Wu, D.-Y.; Cronin, L.; Dong, Q.-F. Design and Performance of Rechargeable Sodium Ion Batteries, and Symmetrical Li-Ion Batteries with Supercapacitor-Like Power Density Based upon Polyoxovanadates. *Adv. Energy Mater.* **2018**, *8* (6), 1701021.

(6) Lv, H.; Geletii, Y. V.; Zhao, C.; Vickers, J. W.; Zhu, G.; Luo, Z.; Song, J.; Lian, T.; Musaev, D. G.; Hill, C. L. Polyoxometalate Water Oxidation Catalysts and the Production of Green Fuel. *Chem. Soc. Rev.* **2012**, *41* (22), 7572–7589.

(7) Weinstock, I. A.; Schreiber, R. E.; Neumann, R. Dioxygen in Polyoxometalate Mediated Reactions. *Chem. Rev.* **2018**, *118* (5), 2680–2717.

(8) Tiwari, C. K.; Baranov, M.; Neyman, A.; Neumann, R.; Weinstock, I. A. Selective Oxidation by $H_5[PV_2Mo_{10}O_{40}]$ in a Highly Acidic Medium. *Inorg. Chem.* **2020**, *59* (17), 11945–11952.

(9) Khenkin, A. M.; Weiner, L.; Wang, Y.; Neumann, R. Electron and Oxygen Transfer in Polyoxometalate, $H_5PV_2Mo_{10}O_{40}$, Catalyzed Oxidation of Aromatic and Alkyl Aromatic Compounds: Evidence for Aerobic Mars−van Krevelen-Type Reactions in the Liquid Homogeneous Phase. *J. Am. Chem. Soc.* **2001**, *123* (35), 8531–8542.

(10) Wang, S.-S.; Yang, G.-Y. Recent Advances in Polyoxometalate-Catalyzed Reactions. *Chem. Rev.* **2015**, *115* (11), 4893–4962.

(11) Kamata, K.; Yonehara, K.; Nakagawa, Y.; Uehara, K.; Mizuno, N. Efficient Stereo- and Regioselective Hydroxylation of Alkanes Catalysed by a Bulky Polyoxometalate. *Nat. Chem.* **2010**, *2* (6), 478–483.

(12) Shinachi, S.; Matsushita, M.; Yamaguchi, K.; Mizuno, N. Oxidation of Adamantane with 1 Atm Molecular Oxygen by Vanadium-Substituted Polyoxometalates. *J. Catal.* **2005**, *233* (1), 81–89.
(13) Seki, Y.; Mizuno, N.; Misono, M. Catalytic Performance of 11-Molybdo-1-Vanadophosphoric Acid as a Catalyst Precursor and the Optimization of Reaction Conditions for the Oxidation of Methane with Hydrogen Peroxide. *Appl. Catal. Gen.* **2000**, *194–195*, 13–20.
(14) Domaille, P. J. The 1- and 2-Dimensional Tungsten-183 and Vanadium-51 NMR Characterization of Isopolymetalates and Heteropolymetalates. *J. Am. Chem. Soc.* **1984**, *106* (25), 7677–7687.
(15) Cadot, E.; Thouvenot, R.; Teze, A.; Herve, G. Syntheses and Multinuclear NMR Characterizations of .Alpha.-$[SiMo_2W_9O_{39}]^{8-}$ and .Alpha.-$[SiMo_{3-X}V_xW_9O_{40}]^{(4+x)-}$ (x = 1, 2) Heteropolyoxometalates. *Inorg. Chem.* **1992**, *31* (20), 4128–4133.
(16) Domaille, P. J.; Watunya, G. Synthesis and Tungsten-183 NMR Characterization of Vanadium-Substituted Polyoxometalates Based on B-Type Tungstophosphate $PW_9O_{34}^{9-}$ Precursors. *Inorg. Chem.* **1986**, *25* (8), 1239–1242.
(17) Finke, R. G.; Rapko, Brian.; Saxton, R. J.; Domaille, P. J. Trisubstituted Heteropolytungstates as Soluble Metal Oxide Analogs. III. Synthesis, Characterization, Phosphorus-31, Silicon-29, Vanadium-51, and 1- and 2-D Tungsten-183 NMR, Deprotonation, and Proton Mobility Studies of Organic Solvent Solute Forms of $H_xSiW_9V_3O_{40}^{x-7}$ and $H_xP_2W_{15}V_3O_{62}^{x-9}$. *J. Am. Chem. Soc.* **1986**, *108* (11), 2947–2960.
(18) Leparulo-Loftus, M. A.; Pope, M. T. Vanadium-51 NMR Spectroscopy of Tungstovanadate Polyanions. Chemical Shift and Line-Width Patterns for the Identification of Stereoisomers. *Inorg. Chem.* **1987**, *26* (13), 2112–2120.
(19) Canny, Jacqueline.; Thouvenot, Rene.; Teze, Andre.; Herve, Gilbert.; Leparulo-Loftus, Michele.; Pope, M. T. Disubstituted Tungstosilicates. 2. .Gamma.- and .Beta.-Isomers of Tungstovanadosilicate, $[SiV_2W_{10}O_{40}]^{6-}$: Syntheses and Structure Determinations by Tungsten-183, Vanadium-51 and Silicon-29 NMR Spectroscopy. *Inorg. Chem.* **1991**, *30* (5), 976–981.
(20) Smith, D. P.; Pope, M. T. Heteropoly 12-Metallophosphates Containing Tungsten and Vanadium. Preparation, Voltammetry, and Properties of Mono-, Di-, Tetra-, and Hexavanado Complexes. *Inorg. Chem.* **1973**, *12* (2), 331–336.
(21) Mialane, P.; Marrot, J.; Rivière, E.; Nebout, J.; Hervé, G. Structural Characterization and Magnetic Properties of Sandwich-Type Tungstoarsenate Complexes. Study of a Mixed-Valent V^{IV}_2/V^V Heteropolyanion. *Inorg. Chem.* **2001**, *40* (1), 44–48.
(22) Drewes, D.; Limanski, E. M.; Piepenbrink, M.; Krebs, B. Neue Heteropolyanionen des Wolframs mit Vanadium(IV) als Heteroatom. *Z. Für Anorg. Allg. Chem.* **2004**, *630* (1), 58–62.
(23) Yamase, T.; Botar, B.; Ishikawa, E.; Fukaya, K. Chemical Structure and Intramolecular Spin-Exchange Interaction of $[(VO)_3(SbW_9O_{33})]^{12-}$. *Chem. Lett.* **2001**, *30* (1), 56–57.
(24) Botar, B.; Yamase, T.; Ishikawa, E. Synthesis and Crystal Structure of a Novel Vanadium-Containing Tungstobismutate(III) $K_{12}[(VO)_3(BiW_9O_{33})_2]\cdot 30H_2O$. *Inorg. Chem. Commun.* **2001**, *4* (10), 551–554.
(25) Xu, Z.-H.; Liu, J.; Wang, E.-B.; Qin, C.; Wu, Q.; Shi, Q. Synthesis, Characterization and Crystal Structure of a Novel Vanadium-Substituted Polyoxometalate Based on the $[BiW_9O_{33}]^{9-}$ Units. *J. Mol. Struct.* **2008**, *873* (1), 41–45.

(26) Joo, N.; Hossu, M.; Rusu, D.; Marcu, A.; Rusu, M.; Pasca, C.; David, L. Synthesis and Physical-Chemical Study of Two Sandwich-Type Heteropolyoxometalates with Dinuclear Vanadium Clusters. *Acta Chim. Slov.* **2007**, *54* (4), 749–754.

(27) Abramov, P. A.; Peresypkina, E. V.; Izarova, N. V.; Vicent, C.; Zhdanov, A. A.; Kompankov, N. B.; Gutsul, T.; Sokolov, M. N. Polyoxoanions Assembled by the Condensation of Vanadate, Tungstate and Selenite: Solution Studies and Crystal Structures of the Mixed Metal Derivatives $(NMe_4)_2Na_2[W^{VI}_4V^{V}_2O_{19}]\cdot 8H_2O$ and $(NMe_4)_{4.83}[(Se^{IV}W^{VI}_{4.57}V^{V}_{4.43}O_{33})_2(W^{VI}(O)(H_2O))(V^{V}O)_{2.6}]\cdot 10.57H_2O$. *New J. Chem.* **2016**, *40* (2), 937–944.

(28) Botar, B.; Yamase, T.; Ishikawa, E. A Highly Nuclear Vanadium-Containing Tungstobismutate: Synthesis and Crystal Structure of $K_{11}H[(BiW_9O_{33})_3Bi_6(OH)_3(H_2O)_3V_4O_{10}]\cdot 25H_2O$. *Inorg. Chem. Commun.* **2000**, *3* (11), 579–584.

(29) Corella-Ochoa, M. N.; Miras, H. N.; Kidd, A.; Long, D.-L.; Cronin, L. Assembly of a Family of Mixed Metal {Mo : V} Polyoxometalates Templated by TeO_3^{2-}: $\{Mo_{12}V_{12}Te_3\}$, $\{Mo_{12}V_{12}Te_2\}$ and $\{Mo_{17}V_8Te\}$. *Chem. Commun.* **2011**, *47* (31), 8799–8801.

(30) Müller, A.; Pope, M. T.; Merca, A.; Bögge, H.; Schmidtmann, M.; van Slageren, J.; Dressel, M.; Kurth, D. G. A Small Cavity with Reactive Internal Shell Atoms Spanned by Four $\{As(W/V)_9\}$-Type Building Blocks Allows Host–Guest Chemistry under Confined Conditions. *Chem. – Eur. J.* **2005**, *11* (20), 5849–5854.

(31) Hervé, G.; Tézé, A.; Contant, R. General Principles of The Synthesis of Polyoxometalates in Aqueous Solution. In *Polyoxometalate Molecular Science*; Borrás-Almenar, J. J., Coronado, E., Müller, A., Pope, M., Eds.; NATO Science Series; Springer Netherlands: Dordrecht, 2003; pp 33–54.

(32) Robert, F.; Leyrie, M.; Hervé, G. Structure of Potassium Diaquatricuprooctadecatungstodiarsenate(III)(12–) Undecahydrate. *Acta Crystallogr. B* **1982**, *38* (2), 358–362.

(33) Kortz, U.; Al-Kassem, N. K.; Savelieff, M. G.; Al Kadi, N. A.; Sadakane, M. Synthesis and Characterization of Copper-, Zinc-, Manganese-, and Cobalt-Substituted Dimeric Heteropolyanions, $[(\alpha\text{-}XW_9O_{33})_2M_3(H_2O)_3]^{n-}$ (n = 12, X = As^{III}, Sb^{III}, M = Cu^{2+}, Zn^{2+}; n = 10, X = Se^{IV}, Te^{IV}, M = Cu^{2+}) and $[(\alpha\text{-}AsW_9O_{33})_2WO(H_2O)M_2(H_2O)_2]^{10-}$ (M = Zn^{2+}, Mn^{2+}, Co^{2+}). *Inorg. Chem.* **2001**, *40* (18), 4742–4749.

(34) Kortz, U.; Nellutla, S.; Stowe, A. C.; Dalal, N. S.; van Tol, J.; Bassil, B. S. Structure and Magnetism of the Tetra-Copper(II)-Substituted Heteropolyanion $[Cu_4K_2(H_2O)_8(\alpha\text{-}AsW_9O_{33})_2]^{8-}$. *Inorg. Chem.* **2004**, *43* (1), 144–154.

(35) Bösing, M.; Nöh, A.; Loose, I.; Krebs, B. Highly Efficient Catalysts in Directed Oxygen-Transfer Processes: Synthesis, Structures of Novel Manganese-Containing Heteropolyanions, and Applications in Regioselective Epoxidation of Dienes with Hydrogen Peroxide. *J. Am. Chem. Soc.* **1998**, *120* (29), 7252–7259.

(36) Bi, L.-H.; Reicke, M.; Kortz, U.; Keita, B.; Nadjo, L.; Clark, R. J. First Structurally Characterized Palladium(II)-Substituted Polyoxoanion: $[Cs_2Na(H_2O)_{10}Pd_3(\alpha\text{-}Sb^{III}W_9O_{33})_2]^{9-}$. *Inorg. Chem.* **2004**, *43* (13), 3915–3920.

(37) Merca, A.; Müller, A.; van Slageren, J.; Läge, M.; Krebs, B. Systematic Study of the Interaction Between V^{IV} Centres and Lanthanide Ions MIII in Well Defined $\{V^{IV}_2M^{III}\}\{As^{III}W_9O_{33}\}_2$ Sandwich Type Clusters: Part 1. *J. Clust. Sci.* **2007**, *18* (3), 711–719.

(38) Merca, A.; Schnack, J.; van Slageren, J.; Glaser, T.; Bögge, H.; Hoeke, V.; Läge, M.; Müller, A.; Krebs, B. Systematic Study of the Interaction Between V^{IV} Centres and Ln^{III} Ions in Well Defined $\{V_2^{IV}Ln^{III}\}\{As^{III}W_9O_{33}\}_2$ Sandwich-Type Clusters: Part 2. *J. Clust. Sci.* **2013**, *24* (4), 979–988.

(39) Wang, K.-Y.; Bassil, B. S.; Xing, X.; Keita, B.; Bindra, J. K.; Diefenbach, K.; Dalal, N. S.; Kortz, U. Incorporation of Transition-Metal-Ion Guests (Co^{2+}, Ni^{2+}, Cu^{2+}, Zn^{2+}) into the Ti_2-Containing 18-Tungsto-2-Arsenate(III) Monolacunary Host. *Eur. J. Inorg. Chem.* **2016**, *2016* (36), 5519–5529.

(40) Yang, P.; Lin, Z.; Bassil, B. S.; Alfaro-Espinoza, G.; Ullrich, M. S.; Li, M.-X.; Silvestru, C.; Kortz, U. Tetra-Antimony(III)-Bridged 18-Tungsto-2-Arsenates(V), $[(LSb^{III})_4(A\text{-}\alpha\text{-}As^{V}W_9O_{34})_2]^{10-}$ (L = Ph, OH): Turning Bioactivity On and Off by Ligand Substitution. *Inorg. Chem.* **2016**, *55* (8), 3718–3720.

(41) Shmakova, A. A.; Romanova, T. E.; Kompankov, N. B.; Abramov, P. A.; Sokolov, M. N. Trapping of NbV by $XW_9O_{33}^{9-}$ (X = As, Sb): Formation of New Sandwich-Type POM Complexes and Their Solution Behavior. *Eur. J. Inorg. Chem.* **2019**, *2019* (20), 2543–2548.

(42) Jeannin, Y.; Martin-Frere, J. Tungsten-183 NMR and x-Ray Study of a Heteropolyanion $[As_2W_{21}O_{69}(H_2O)]^{6-}$ Exhibiting a Rare Square-Pyramidal Environment for Some Tungsten(VI). *J. Am. Chem. Soc.* **1981**, *103* (7), 1664–1667.

(43) Yamase, T.; Ishikawa, E.; Fukaya, K.; Nojiri, H.; Taniguchi, T.; Atake, T. Spin-Frustrated $(VO)_3^{6+}$-Triangle-Sandwiching Octadecatungstates as a New Class of Molecular Magnets. *Inorg. Chem.* **2004**, *43* (25), 8150–8157.

(44) Kohama, Y.; Kawaji, H.; Atake, T.; Fukaya, K.; Yamase, T. Low-Temperature Heat Capacity of Triangle Antiferromagnetic Molecular Clusters $K_{12}[(VO)_3(SbW_9O_{33})_2]\cdot 15H_2O$ and $K_{12}[(VO)_3(BiW_9O_{33})_2]\cdot 29H_2O$. *J. Solid State Chem.* **2009**, *182* (6), 1468–1472.

(45) Yamase, T.; Botar, B.; Ishikawa, E.; Fukaya, K.; Shigeta, S. Magnetic Exchange Coupling and Potent Antiviral Activity of $[(VO)_3(SbW_9O_{33})_2]^{12-}$ in *Polyoxometalate chemistry for nanocomposite design*. Dordrecht: Kluwer; **2002**.

(46) Shigeta, S.; Mori, S.; Kodama, E.; Kodama, J.; Takahashi, K.; Yamase, T. Broad Spectrum Anti-RNA Virus Activities of Titanium and Vanadium Substituted Polyoxotungstates. *Antiviral Res.* **2003**, *58* (3), 265–271.

(47) Tourné, C.; Tourné, G. Les 19-tungstodimétallo-diarséniates (III). Etude préliminaire. *C. R. Acad. Sci. Paris* **1975**, *281*, 933.

(48) Bösing, M.; Loose, I.; Pohlmann, H.; Krebs, B. New Strategies for the Generation of Large Heteropolymetalate Clusters: The β-B-SbW_9 Fragment as a Multifunctional Unit. *Chem. – Eur. J.* **1997**, *3* (8), 1232–1237.

(49) Dolomanov, O. V.; Bourhis, L. J.; Gildea, R. J.; Howard, J. a. K.; Puschmann, H. OLEX2: A Complete Structure Solution, Refinement and Analysis Program. *J. Appl. Crystallogr.* **2009**, *42* (2), 339–341.

(50) Sheldrick, G. M. SHELXT – Integrated Space-Group and Crystal-Structure Determination. *Acta Crystallogr. Sect. Found. Adv.* **2015**, *71* (1), 3–8.

(51) Sheldrick, G. M. Crystal Structure Refinement with SHELXL. *Acta Crystallogr. Sect. C Struct. Chem.* **2015**, *71* (1), 3–8.

(52) Altenau, J. J.; Pope, M. T.; Prados, R. A.; So, Hyunsoo. Models for Heteropoly Blues. Degrees of Valence Trapping in Vanadium(IV)- and Molybdenum(V)-Substituted Keggin Anions. *Inorg. Chem.* **1975**, *14* (2), 417–421.

(53) Brown, I. D.; Altermatt, D. Bond-Valence Parameters Obtained from a Systematic Analysis of the Inorganic Crystal Structure Database. *Acta Crystallogr. B* **1985**, *41* (4), 244–247.
(54) Haouas, M.; Mbomekallé, I.-M.; Vila, N.; de Oliveira, P.; Taulelle, F. ^{183}W INADEQUATE 2D NMR Spectroscopy of Hetero Arsenato–Phosphato–Tungstate P^{V}/As^{V} Substitution in Dawson-Type α-$[As_xP_{2-X}W_{18}O_{62}]^{6-}$ (x = 0–2) and α-$[H_4As_yP_{1-Y}W_{18}O_{62}]^{7-}$ (y = 0, 1). *Inorg. Chem.* **2014**, *53* (11), 5568–5574.
(55) Fedotov, M. A.; Maksimovskaya, R. I. NMR Structural Aspects of the Chemistry of V, Mo, W Polyoxometalates. *J. Struct. Chem.* **2006**, *47* (5), 952–978.
(56) Andersson, I.; Hastings, J. J.; Howarth, O. W.; Pettersson, L. Aqueous Tungstovanadate Equilibria. *J. Chem. Soc. Dalton Trans.* **1996**, No. 13, 2705–2711.

SYNOPSIS

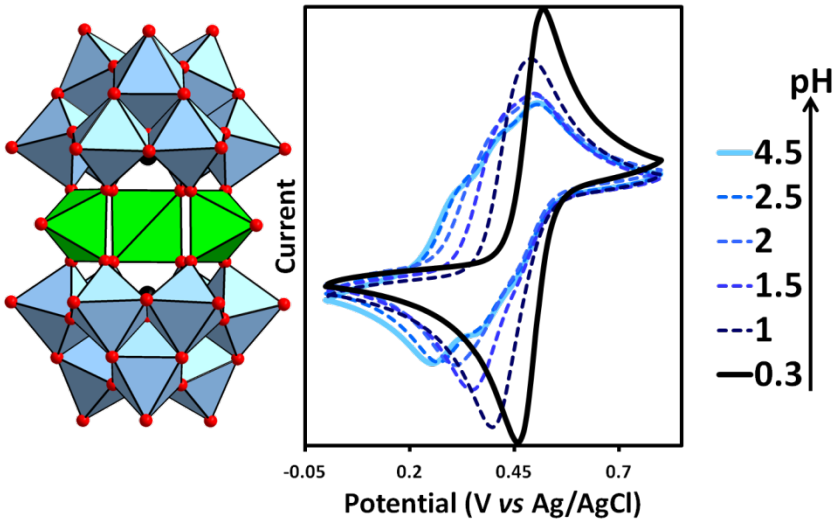

We report the electrochemical preparation and structural characterizations (^{17}O, ^{51}V, and ^{183}W NMR and X-ray diffraction) of the fully oxidized V^{V} containing polyanions $[(VO)_3(XW_9O_{33})_2]^{9-}$ with X = As^{III} or Sb^{III}. Electrochemical studies reveal the three vanadium centers undergo one-electron transfer through pH-dependent processes. Remarkably, this polyoxometalate exhibits a single quasi-reversible redox wave corresponding to a 3e-/3H^+ proton-coupled-electron-transfer (PCET) in acidic conditions.